The influence of abrupt changes in the cross-sectional area of a railway tunnel on the propagation of pressure waves caused by passing trains

Ottitsch F., Sockel H., Peiffer A.
Institut für Strömungslehre und Wärmeübertragung
Technische Universität Wien, Wiedner Hauptstr. 7 A-1040 Wien

Abstract

In modern railway tunnels we can find sudden changes in the cross-sectional area along the tunnel axis. In this paper the effect of such changes on the propagation of pressure waves through the tunnel is investigated in a local region of the size of the tunnel diameter D_T^* (small scale) and in the region of the size of the tunnel length L_T^* (large scale).

It is shown that locally radial moving pressure waves originate at the jumps which propagate along the tunnel axis. If the length of the primary pressure wave front is of the order or smaller than the tunnel diameter, the amplitudes of these radial waves can be of the order of the reflected plane waves. But the usual theory for one-dimensional unsteady flow does still give a good estimate of the flow field, because these radial waves do not transport mass or momentum as a first order approximation shows (see [4]).

Concerning the whole tunnel these changes in the cross-sectional area lead to secondary waves propagating superimposed on the primary waves. If the jumps of the cross-section are not taken into account in a mathematical model, the comparison between measured and calculated data will be poor. It is shown that an area jump can be simulated with the assumption of a smoothly varying cross-section. However this assumption introduces an error in the phasing of the secondary waves of the order of the grid-size.

Nomenclature

Latin Symbols

A^*	local cross-sectional area of the tunnel
a_0^*, a^*, a	undisturbed speed of sound, speed of sound, dimensionless speed of sound
D_T^*	tunnel diameter
L_T^*	tunnel length
p^*, p_0^*, p	pressure, undisturbed pressure, dimensionless pressure

r^*, r	coordinate in radial direction, dimensionless coordinate
t^*, t	time, dimensionless time
u^*, u	fluid velocity in radial direction, dimensionless velocity
U^*	local cross-sectional perimeter of the tunnel
w^*, w	fluid velocity in axial direction, dimensionless velocity
z^*, z	coordinate in axial direction, dimensionless coordinate

Greek Symbols

ρ^*, ρ_0^*, ρ	density, undisturbed density, dimensionless density
κ	isentropic exponent
Φ	velocity potential
τ^*	wall friction
$\triangle r$, $\triangle t$, $\triangle z$	grid size in r, t and z-direction

1 Introduction

The conventional method of calculating the flow inside of railway tunnels consists of an one-dimensional approach (see for instance [9]). It is possible, to apply this method to tunnels with smoothly varying tunnel areas. In this theory the flow field inside the tunnel is coupled with special boundary conditions to the flow in the region of the train and outside the tunnel. This theory is of course only a model of reality and like any good model it involves important simplifications compared to the real flow. Possible reasons for discrepancies are experimental errors, errors influencing the conservation laws and errors in the way the train/tunnel system is modelled.

This paper deals with sudden changes of the tunnel cross-sections, a frequent case where the representation of the tunnel system loses accuracy. In another paper [4] the modelling of the train ends as sudden changes in area is investigated.

In modern German railway tunnels abrupt changes in the cross-sectional area (approx. between 81,0 - 98,0 m^2) occur. The effects of such sudden changes in the cross-section can be investigated in a local region of the size of the tunnel diameter D_T^* (small scale) and in a region of the size of the tunnel length L_T^* (large scale). This and the knowledge, that pressure and velocity disturbances propagate approximately at the speed of sound a_0^* (relative to the fluid) leads to two different characteristic time scales for the unsteady flow field. For the local region the time scale that has to be investigated is D_T^*/a_0^* and for the whole tunnel it is L_T^*/a_0^*. Obviously in the small scale an error in the representation of the geometry of the train/tunnel system will be more important than errors in the conservation of mass, momentum and energy. On the other hand for the large region the correct representation of the geometry (besides the right cross-sectional area) will be of less importance compared to errors in the conservation laws.

2 Local Effects

2.1 Theory

If one attempts to simulate the fluid flow inside a tunnel in a local region it seems quite obvious to neglect heat and mass transfers along the tunnel walls. Furthermore due to the relative small effect of friction even on the flow in the whole tunnel there is no need to include friction effects in such a model. A fairly good approximation of the tunnel geometry is a semi-circular tube which has an abrupt change in cross-section at $z = 0$ (see figure 1).

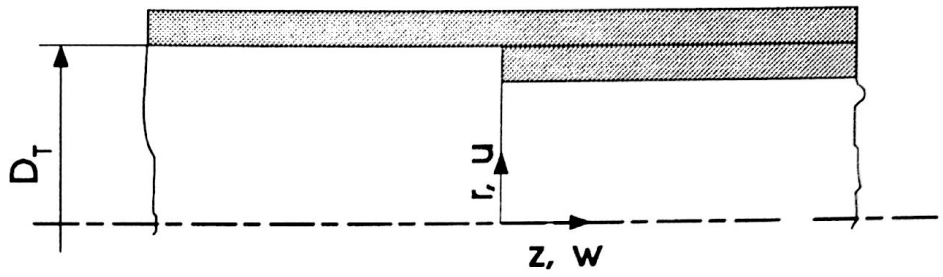

Figure 1: Geometry of tunnel

We assume small pressure fluctuations in a compressible, isentropic, cylindrical flow field.

Euler-equation in radial direction:

$$\frac{\partial u^*}{\partial t^*} + u^* \frac{\partial u^*}{\partial r^*} + w^* \frac{\partial u^*}{\partial z^*} = -\frac{1}{\rho^*} \frac{\partial p^*}{\partial r^*} \tag{1}$$

Euler-equation in axial direction:

$$\frac{\partial w^*}{\partial t^*} + u^* \frac{\partial w^*}{\partial r^*} + w^* \frac{\partial w^*}{\partial z^*} = -\frac{1}{\rho^*} \frac{\partial p^*}{\partial z^*} \tag{2}$$

Continuity equation:

$$\frac{\partial \rho^*}{\partial t^*} + u^* \frac{\partial \rho^*}{\partial r^*} + w^* \frac{\partial \rho^*}{\partial z^*} + \rho^* \frac{\partial u^*}{\partial r^*} + \rho^* \frac{\partial w^*}{\partial z^*} + \frac{\rho^* u^*}{r^*} = 0 \tag{3}$$

with the equation for the isentropic speed of sound

$$\frac{\partial \rho^*}{\partial p^*} = \frac{1}{a^{*2}} \tag{4}$$

equation 3 yields

$$\frac{1}{\rho^* a^{*2}}\frac{\partial p^*}{\partial t^*} + \frac{u^*}{\rho^* a^{*2}}\frac{\partial p^*}{\partial r^*} + \frac{w^*}{\rho^* a^{*2}}\frac{\partial p^*}{\partial z^*} + \frac{\partial u^*}{\partial r^*} + \frac{\partial w^*}{\partial z^*} + \frac{u^*}{r^*} = 0 \tag{5}$$

By introducing the dimensionless quantities

$$u = \frac{u^*}{a_0^*} \quad w = \frac{w^*}{a_0^*} \quad r = \frac{r^*}{D_T^*} \quad z = \frac{z^*}{D_T^*} \quad t = \frac{t^* a_0^*}{D_T^*} \quad p = \frac{p^* - p_0^*}{\rho_0^* a_0^{*2}} \quad \rho = \frac{\rho^*}{\rho_0^*} \quad a = \frac{a^*}{a_0^*}$$

we get from the equations 1, 2 and 5

$$\frac{\partial u}{\partial t} + u\frac{\partial u}{\partial r} + w\frac{\partial u}{\partial z} = -\left(\frac{1}{1+\kappa p}\right)^{\frac{1}{\kappa}}\frac{\partial p}{\partial r} \tag{6}$$

$$\frac{\partial w}{\partial t} + u\frac{\partial w}{\partial r} + w\frac{\partial w}{\partial z} = -\left(\frac{1}{1+\kappa p}\right)^{\frac{1}{\kappa}}\frac{\partial p}{\partial z} \tag{7}$$

$$\frac{\partial p}{\partial t} = -u\frac{\partial p}{\partial r} - w\frac{\partial p}{\partial z} - (1+\kappa p)\left(\frac{\partial u}{\partial r} + \frac{\partial w}{\partial z} + \frac{u}{r}\right) \tag{8}$$

If one restricts these equations to small scales (z of the order of several tunnel diameters) and to small disturbances ($p \ll 1$) then these equations can be linearized and finally gives:

$$\frac{\partial u}{\partial t} = -\frac{\partial p}{\partial r} \tag{9}$$

$$\frac{\partial w}{\partial t} = -\frac{\partial p}{\partial z} \tag{10}$$

$$\frac{\partial p}{\partial t} = -\frac{\partial u}{\partial r} - \frac{\partial w}{\partial z} - \frac{u}{r} \tag{11}$$

By introducing the potential Φ with

$$u = \frac{\partial \Phi}{\partial r} \quad w = \frac{\partial \Phi}{\partial z} \quad p = -\frac{\partial \Phi}{\partial t}$$

One can derive the well known wave equation and get interesting results concerning the principal behaviour of solutions inside a tunnel [4]. In this paper it is shown, that periodic waves propagating in tangential or radial direction exist, and that for each wave mode there exists a so called cutoff-frequency below which this mode cannot propagate. These so called higher mode waves do neither transport mass nor momentum in a first order approximation.

Another possible way of solving the equations (9), (10) and (11) is by means of numerical methods. In [2] several numerical methods have been compared with each other by the use of an analytical test case regarding accuracy, computing effort, CPU-time and mass storage. The outcome of this work was, that a good choice for

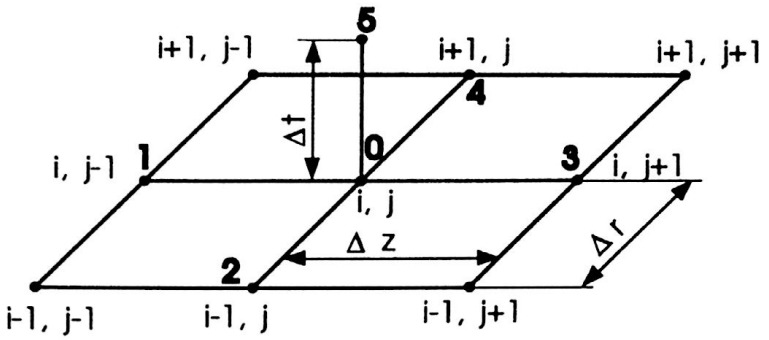

Figure 2: Numerical grid

a difference formulation, which is likely to give a correct result for waves travelling in radial and axial directions, would be a McCormick scheme. Therefore the above equations were calculated with a two step Predictor–Corrector Scheme (see figure 2 for the numerical grid):

Predictor

$$u_0^{(p)} = u_0 - \frac{\Delta t}{\Delta r}(p_4 - p_0) \tag{12}$$

$$w_0^{(p)} = w_0 - \frac{\Delta t}{\Delta z}(p_3 - p_0) \tag{13}$$

$$p_0^{(p)} = p_0 - \frac{\Delta t}{\Delta r}(u_4 - u_0) - \frac{\Delta t}{\Delta z}(w_3 - w_0) - \frac{u_0 \Delta t}{r} \tag{14}$$

Corrector

$$u_5 = \frac{1}{2}\left[u_0 + u_0^{(p)} - \frac{\Delta t}{\Delta r}(p_0 - p_2)\right] \tag{15}$$

$$w_5 = \frac{1}{2}\left[w_0 + w_0^{(p)} - \frac{\Delta t}{\Delta z}(p_0 - p_1)\right] \tag{16}$$

$$p_5 = \frac{1}{2}\left[p_0 + p_0^{(p)} - \frac{\Delta t}{\Delta r}(u_0 - u_2) - \frac{\Delta t}{\Delta z}(w_0 - w_1) - \frac{u_0 \Delta t}{r}\right] \tag{17}$$

2.1.1 Range of validity

In the above formulation of the problem several simplifications have been made which will cause differences between the solution of the equations and the real flow field, which will increase with time.

Among other features neglected the most important seem to be:

- Steepening of the wavefront due to $\frac{d(\rho a)}{\rho d\rho} > 0$
- Flattening of wavefront due to unsteady friction or damping effects caused by ballasted tracks
- pressure losses at cross-sectional area changes
- wrong geometric boundary-conditions

Regarding the steepening effect due to a nonlinear theory it has been shown by [9], that these nonlinear effects are unimportant over the large scale of the tunnel length. Therefore it seems to be a good estimate to neglect these influences.

The flattening of a wavefront due to unsteady friction has been investigated in [5]. There it is shown, that this effect is small on a large scale. Furthermore effects like the mass transport in the ballasted track have been noticed by [3]. But these effects became important for large distances (several kilometers) only.

At the cross-sectional jumps pressure losses will occur but they will have only a minor influence on the results. The main focus of this project was to get a first insight into the multidimensional effects.

The boundary conditions applied in the above theory are of course different from those of a tunnel, because the real cross-section is no semi-circle. But as our experiments have shown, this is not important, if the real cross-section is approximately a semi-circle.

2.2 Experiments

A reduced scale tunnel model has been built at the institute. The whole experimental setup is described in principle in [4] and in full detail in [8] and a Dissertation to be published by Ottitsch.

With a pressure wave generator pressure waves can be induced in a tunnel of 7.5 m length and 0.21 m diameter. For a full–scale tunnel with a diameter of 15.12 m this would give a scale factor of 1:72. It is possible to get differential pressure waves between 0 – 1400 Pa with this facility.

Pressure measurements can be made at up to eight different points with a total sampling frequency of 130 kHz. It was possible to get a resolution of approximately 5 Pa.

The primary purpose of the experiments was to check the numerical results.

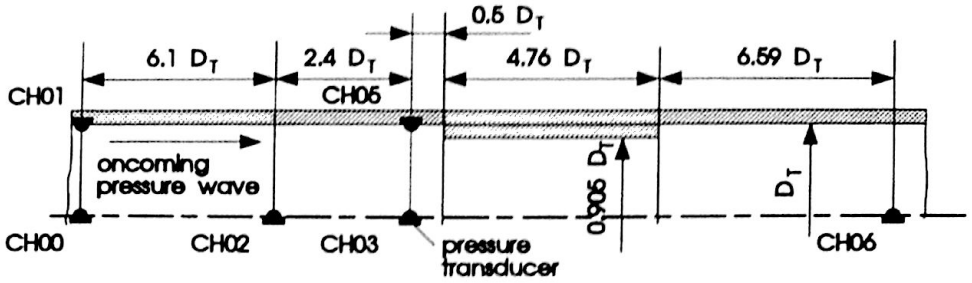

Figure 3: Experimental setup for comparison

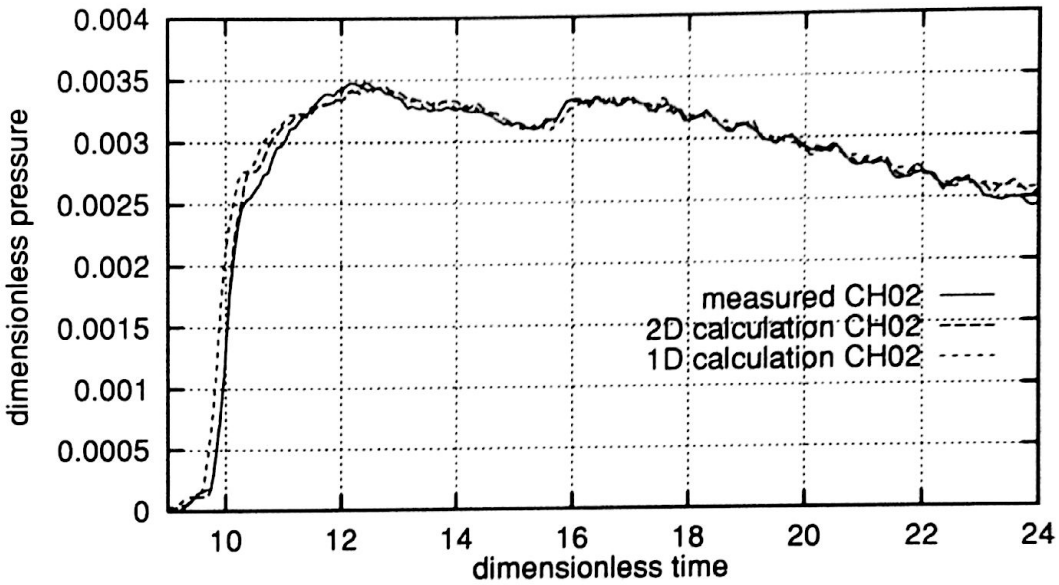

Figure 4: Comparison 1D- and 2D-Calculations vs. experiments CH02

2.3 Results

For all experiments the reference pressure p_0^* was the ambient pressure in the laboratory. In figure 3 one can see the main section of the model tunnel. A pressure wave moves over a section of $1m$ length where the diameter of the tunnel model changes from $0.21m$ to $0.19m$. The pressure histories have been measured at four points in the vicinity of the discontinuities. In figures 4, 5, 6 and 7 one can see comparisons of measured and calculated pressure histories.

To get an initial condition for the calculations the pressure history was measured 9 tunnel diameters ahead of the jump in the cross-section. Due to the fact, that the oncoming wave was not totally plane, this initial condition was strictly not

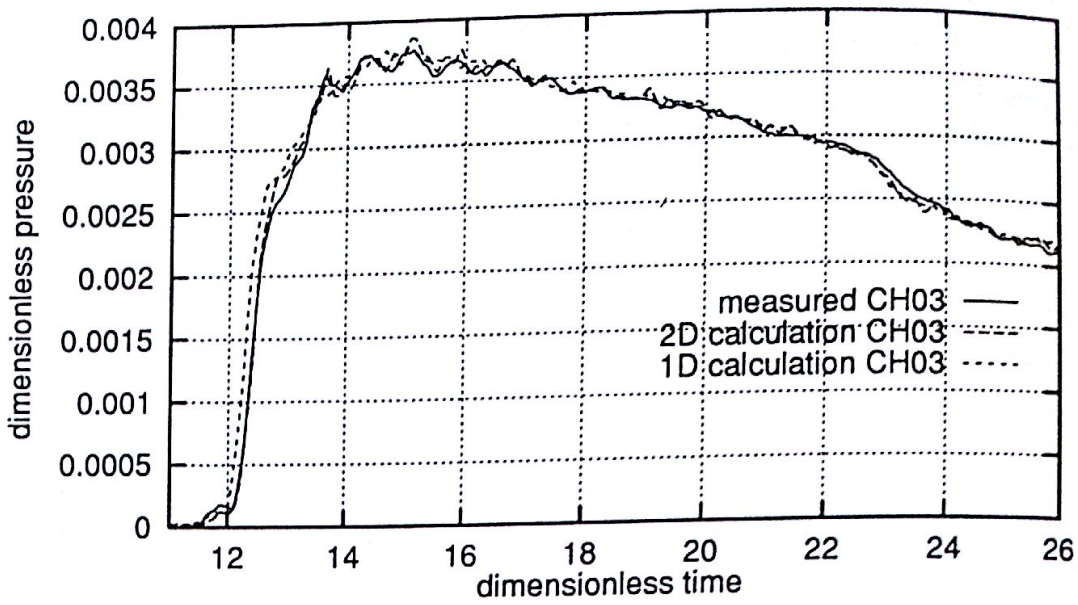

Figure 5: Comparison 1D-and 2D-Calculations vs. experiments CH03

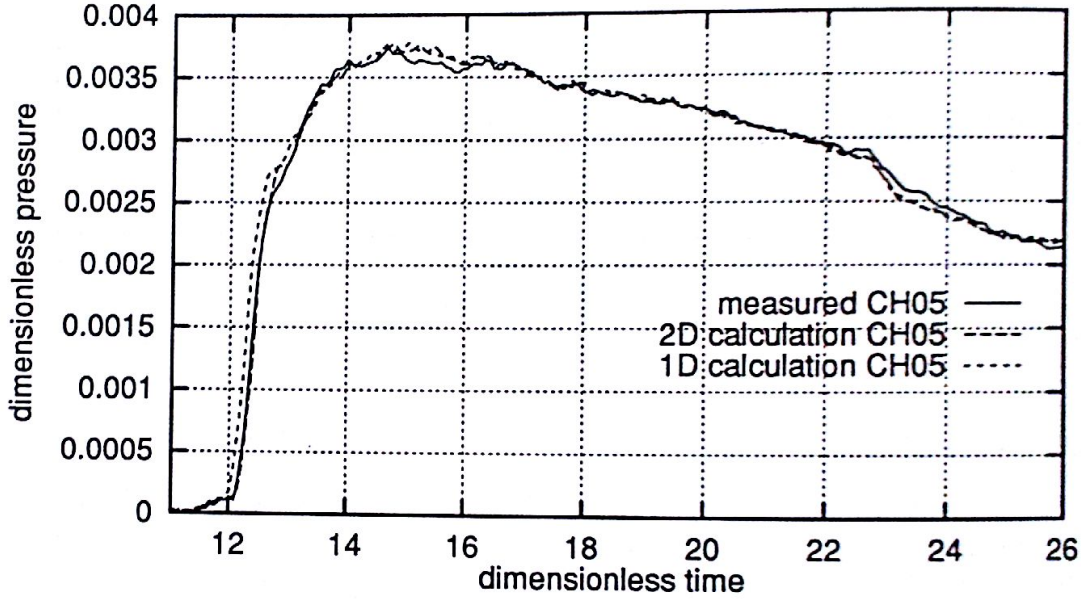

Figure 6: Comparison 1D-and 2D-Calculations vs. experiments CH05

correct. But the coincidence between numerical and experimental results is good, especially concerning the radial propagating waves which are superimposed upon the primary wave. The pressure histories have been calculated applying an usual theory for frictionless one–dimensional flow (see [7]), where the grid size was chosen

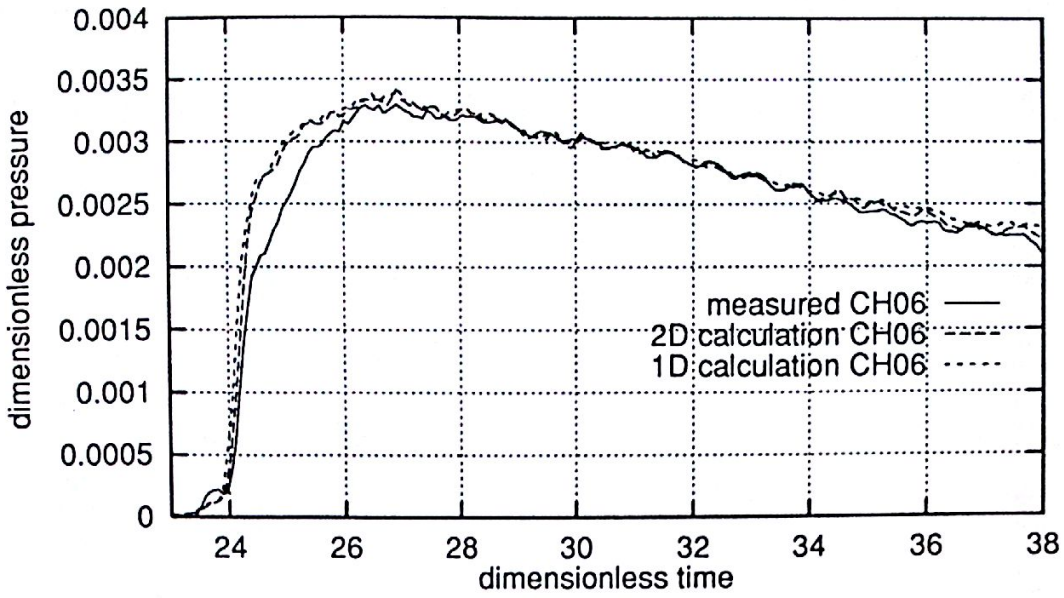

Figure 7: Comparison 1D- and 2D-Calculations vs. experiments CH06

in agreement with the experimental sampling rate. Thus it is possible to see the error caused by such a theory, which cannot simulate the radial moving pressure waves, but gives a good prediction for the overall pressure history. Notice that the pressure history at point CH05 (figure 6) looks almost like a plane wave. This is due to the fact, that the intensity of a radial wave (see figure 5) is rather weak in a point of the perimeter in comparison to a point near the center of the tunnel. It can also be seen that the radial waves propagate slower than the primary wave as can be shown theoretically too (see [4]). Due to the dispersive propagation of these waves they spread out along the tunnel axis and thus the average amplitudes of these waves decrease while propagating along the tunnel. Notice that the shape of the measured primary wave has changed slightly on figure 7 in comparison to the oncoming wave. This is likely to be due to friction effects, which cannot be forecasted with the above theory. Therefore this theory should not be applied to large scales (wave propagating length greater than 20 diameters). However regarding the radial waves the results of the measurements and the calculations agree rather well.

In Figure 8 the calculated pressure distribution inside a duct at different times can be seen. A pressure wave with a nondimensional pressure rising time of 0.25 moves over a discontinuity. At time 0.0 the pressure wave arrives at the discontinuity. In figure 8 low pressure is plotted in dark and high pressure is plotted in bright as shown in the scale to the right. The radial pressure waves are much stronger in the larger duct than in the smaller duct. Furthermore the wavelengths of the radial waves increase with increasing distance from the wave front. This is due to the different group velocities with which each mode propagates when excited at different

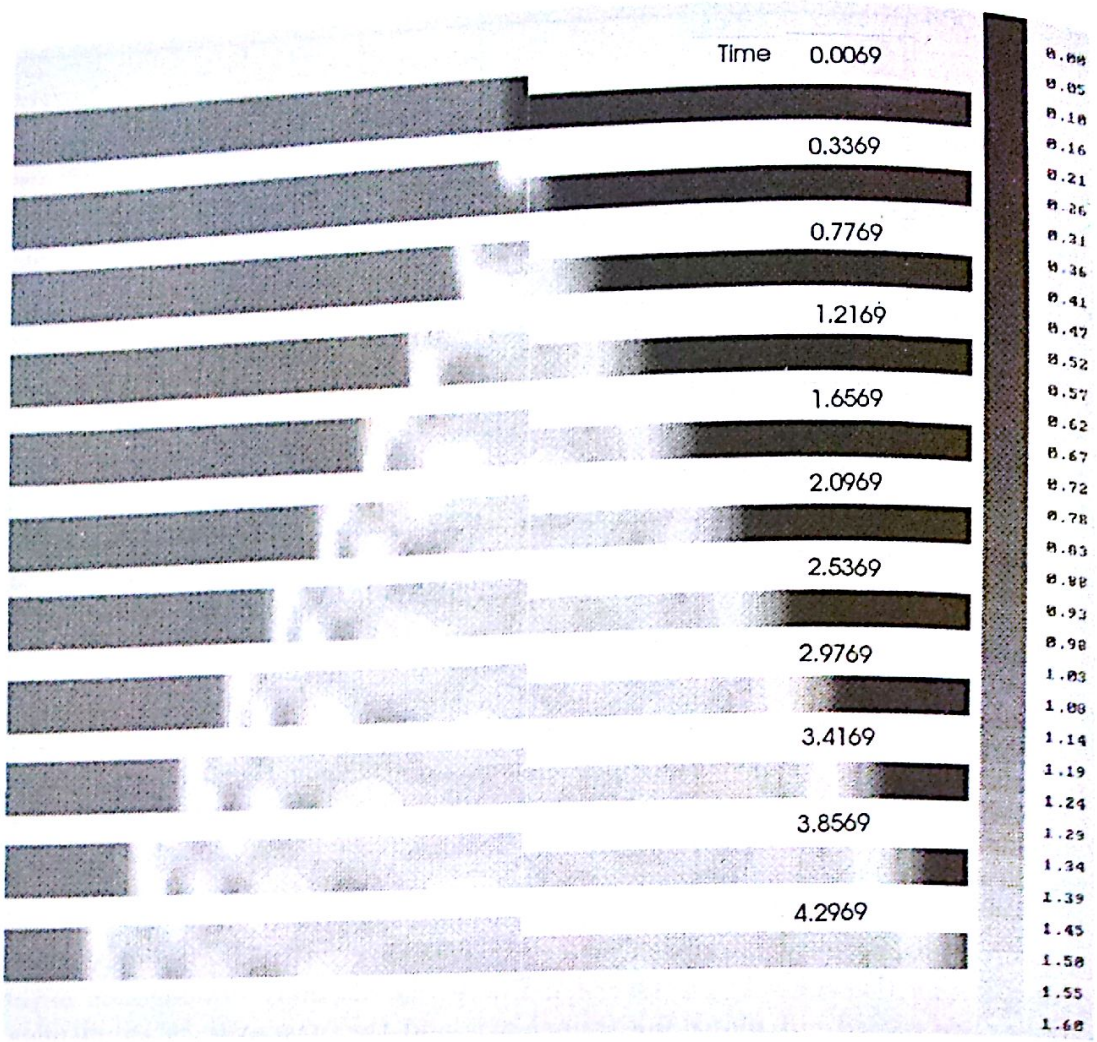

Figure 8: Pressure field at different times

frequencies. (see [4]). The pressure wave that enters the small duct is an almost plane wave, with slightly varying intensity.

The amplitudes of the radial waves are a function of the different radia of the ducts and the pressure rising time. For a short pressure rising time like in the above example the amplitude of a radial wave is of the order of the height of the reflected plane wave.

3 Large scale effects

After having looked at the local effects attention must be payed to the large scale effects. When a pressure wave passes a jump of the cross–sectional area a part of the wave will be reflected back and secondary waves will propagate inside the tunnel. If a theory does not take account of these changes of the cross–sectional area the agreement between calculated and measured pressure histories will be poor.

3.1 Theory

In the conventional approach a discontinuous jump in the cross-sectional area can be modelled with a discontinuity surface. Each discontinuity increases the complexity of a computer program for an otherwise continuous field. Since the pressure losses due to jumps in the cross-section are not important, it is a reasonable assumption to model the jumps as a continuous change.

Under such an assumption the basic equations for one-dimensional, viscous, isentropic flow of a perfect gas in a tunnel with gradually changing cross-sectional area are, if the effect of viscosity is considered in the momentum equation only:

$$\frac{\partial(\rho^* A^*)}{\partial t^*} + \frac{\partial(\rho^* A^* w^*)}{\partial z^*} = 0 \tag{18}$$

$$A^* \frac{\partial w^*}{\partial t^*} + A^* w^* \frac{\partial w^*}{\partial z^*} = -\frac{1}{\rho^*}\frac{\partial p^*}{\partial z^*} - \int_{U^*} \tau^* dU^* \tag{19}$$

$$\frac{dp^*}{p^*} = \kappa \frac{d\rho^*}{\rho^*} \tag{20}$$

There are several ways to model the friction term $\int_{U^*} \tau^* dU^*$ in equation (19). In [5] it is shown, that regarding usual tunnel geometries it is sufficient to use the model of the quasi–steady friction. However it should be pointed out, that there do exist other approaches which model the unsteady friction force too. In the calculations presented in the following section dispersive effects due to the cross–sectional jumps and other influences like unsteady friction and ballasted tracks are taken into account by a numerical damping procedure.

Equations (18) and (19) can be transformed on their characteristics and can then be implemented in a numerical computer program like it is shown for instance in [6].

Here we just mention that one gets compatibility conditions along characteristic lines and discontinuity surfaces as boundary conditions at the train and tunnel ends.

The only new condition is, that the theory does now take into account changes of the cross-sectional area along the tunnel-axis.

3.2 Experiments

	from [m]	to [m]	length [m]	cross-section [m^2]
Northern Portal	0	270	270	81.3
	270	501	231	92.0
	501	930	429	81.3
	930	1656	726	92.0
	165	1810	154	87.0
	1810	2195	385	97.7
	2195	2426	231	87.0
	2426	2767	341	97.7
	2767	2998	231	87.0
	2998	3735	737	97.7
	3735	3966	231	87.0
	3966	4252	286	97.7
	4252	4659	407	81.3
	4659	4890	231	92.0
Southern Portal	4890	5513	623	81.3

Table 1: Cross-sectional area of the Mühlbergtunnel (D)

The german railway organisation DB has much experience in full-scale experiments for tunnel aerodynamics (see for instance [1]). In 1991 this company did some experiments in the Mühlberg-, Sinnberg- and Burgsinner Kuppe–tunnel. Both the Mühlberg- and Sinnbergtunnel have several jumps in the cross-sectional area along the tunnel–axis. In the following section we present the comparison between theory and full–scale experiments for a train passage through the Mühlberg–tunnel.

The train entered the Mühlberg-tunnel at the Southern portal and consisted of an engine of the type 103 (cross-sectional area 10.2 m^2), one testing carriage, another engine of type 120 and eight normal carriages. The overall length was approx. 278 m. The temperature was 7°C. The atmospheric pressure was 986 mbar.

The Mühlberg–tunnel has an overall length of 5513 m. See table 1 for the cross-sectional area along the tunnel axis. Notice that the cross-sectional jump can be as high as 19 %. The average length of a region of constant cross-sectional area is approx. 400 m. This means that one can expect pressure waves with a frequency of approx. 0.4 Hz propagating in the tunnel superimposed upon the signal calculated under the assumption of a constant cross–section.

The pressure measurements were done at three fixed locations inside the tunnel at a distance of 1727 m, 2180 m, 5182 m from the Northern Portal. At each point the pressure was measured at both sides of the tunnel walls. The sampling frequency was approx. 14 Hz. Unfortunately as is shown in [4] the sampling frequency was not high

enough to achieve a satisfying resolution for small scale effects, so that statements regarding the one-dimensionality of the pressure distribution at the tunnel walls must not be made. However regarding large scale effects these measurements are sufficient for a comparison with one–dimensional large scale calculations.

3.3 Results

Preliminary calculations showed that the speed ot the train was not constant while passing the tunnel. But the passing of the train at the points, where the measurements were made, could be identified. The entrance speed could be calculated by the time difference of the entrance of the train nose and tail and the exit time could also be identified. Therefore it was possible to estimate the speed of the train in the tunnel. However it should be pointed out that it remains still some uncertainty about the actual train speed in the experiments. As the height of the primary wave depends on the square of the entrance speed it is recommended that special attention should be given to the actual speed of the train when doing full–scale experiments. However the following approximate train location was deduced from the measurements:

Time [s]	Position [m]
0	0
3.475	278
23.437	1727
29.924	2180
70.61	5182
100.0	7150

For the calculations a train loss-coefficient of 3.7 (see [6] for a definition of the stagnation pressure loss coefficient) was used. The grid width was $45m$ which takes account of the average rising length of the propagating pressure waves.

In the figures 9, 10 and 11 a comparison of the measured and calculated values under the assumption of a constant and a slowly varying cross-section can be seen.

Notice that the results of the calculation with a slowly varying cross-section correspond much better with the experimental results. Especially the superimposed waves caused by the changes of the cross-section are predicted well. But with increasing time the assumption of slowly varying cross-sections leads to a phase error of these waves. This is due to the fact, that the phase error made at each reflection of a superimposed wave is of the order of the grid length.

The comparisons in the figures show, that it is essential to know the variation of the cross–sectional area along the tunnel.

We would like to point out that the good agreement between experimental and numerical results was only possible by taking into account a variable speed of the train deduced from the positions of the trains at different times, which we concluded

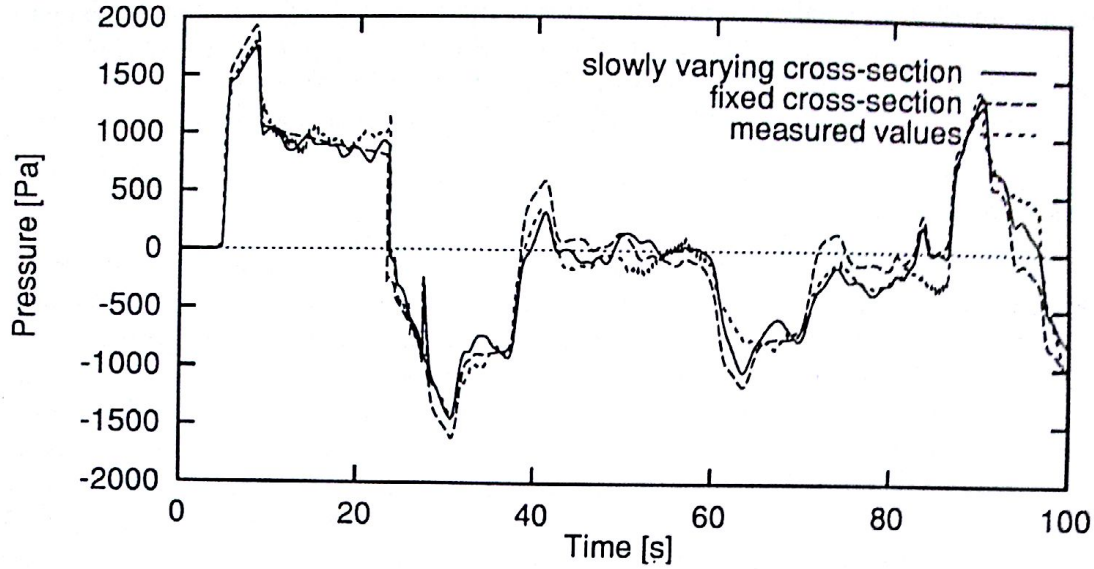

Figure 9: Calculation and Experiment at point 1727 m

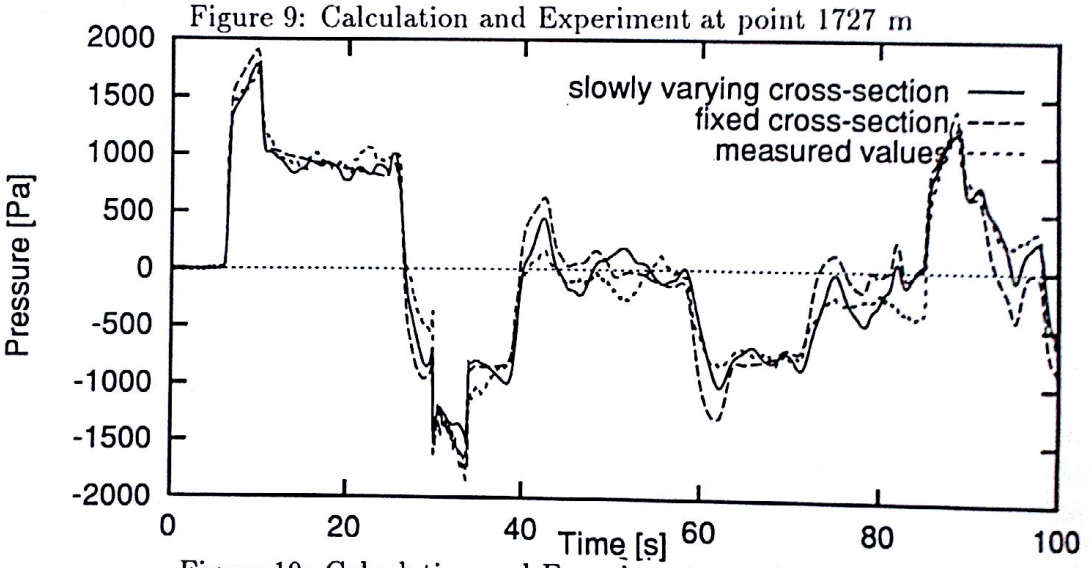

Figure 10: Calculation and Experiment at point 2180 m

from the experiment. Without this measure the agreement between the results was not satisfying.

4 Conclusion

The above described effects on the propagation of pressure waves due to changes in the cross-sectional area of railway tunnels can be simulated on a large scale and a small scale.

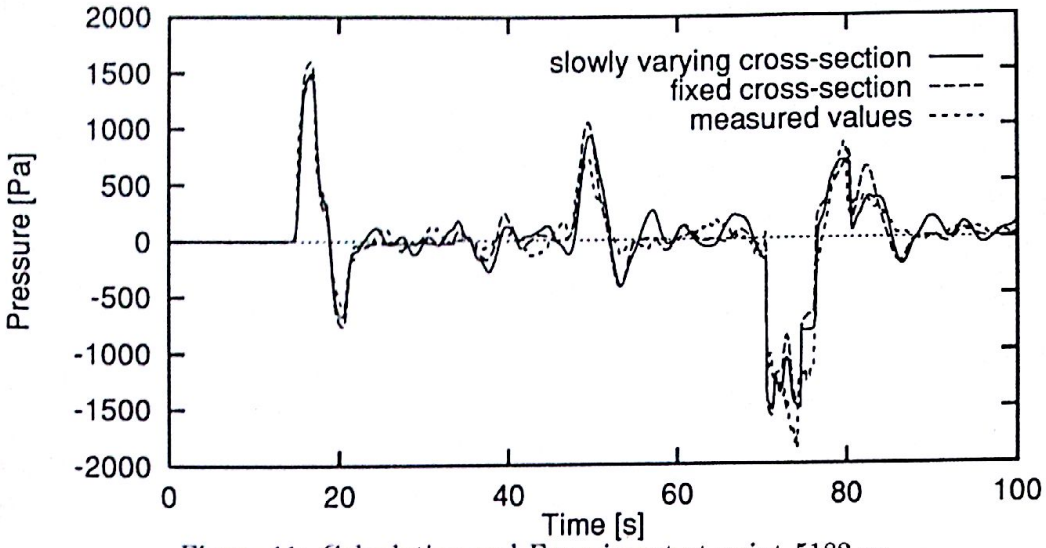

Figure 11: Calculation and Experiment at point 5182 m

Locally these changes produce radial waves which propagate along the tunnel–axis. In the region of the area changes the pressure distribution is nonuniform over the cross–section. However the global pressure history can also be simulated with a theory for an one–dimensional unsteady flow, if the grid–size is choosen smaller than the tunnel diameter, but with such a theory it is not possible to calculate the local pressure maxima and minima due to these radial waves.

When calculating pressure histories for a train passage through a tunnel one has to take into account jumps of the cross–sectional area. Otherwise a good agreement between the theoretical and experimental results cannot be achieved. If a special tunnel has such changes can be detected easily by the secondary waves on the pressure histories of the full-scale experiments. A possible approach to take account of these area jumps is the assumption of a slowly varying cross-section.

Acknowledgements

The authors are very indebted to the German Railway organisation (DB) who performed the full-scale experiments.

References

[1] Glöckle H., Pfretzschner P.: High speed tests with ICE/V passing through tunnels and the effect of sealed coaches on passenger comfort. Proc. 6th Int. Symp. on the Aerodynamics and Ventilation of vehicle tunnels 1988 pp. 23-44

[2] Ottitsch F., Sockel H.: Vergleich von numerischen Verfahren zur Lösung der linearisierten Eulergleichungen. Interner Bericht des Instituts für Strömungslehre TU-Wien 1992

[3] Ozawa S. et. al.: Countermeasures to reduce micro-pressure waves radiating from exits of shinkansen tunnels. Proc. 7th Int. Symp. on the Aerodynamics and Ventilation of Vehicle Tunnels 1991, pp. 253-266

[4] Peiffer A., Ottitsch F., Sockel H.: Experimental and theoretical investigation of two- and three-dimensional pressure waves propagating inside a tunnel due to a train passage. Paper to be published Proc. 8th Int. Symp. on the Aerodynamics and Ventilation of Vehicle Tunnels Liverpool 1994

[5] Schultz M., Sockel H.: The influence of unsteady friction on the propagation of pressure waves in tunnels. Proc. 6th Int. Symp. on the Aerodynamics and Ventilation of vehicle tunnels 1988 pp. 123–135

[6] Sockel H., Waclawiczek M.: Pressure transients and aerodynamic power in railway tunnels with special reference to entropy and air shafts. Proc. 4th Int. Symp. on the Aerodynamics and Ventilation of Vehicle Tunnels, BHRA Fluid Engineering, Cranfield 1982

[7] Sockel H., Ottitsch F.: Numerical and experimental investigation of a pressure measuring system with a restrictor. Journ. on Wind Eng. and Ind. Aerodyn., 41-44 (1992) 975-985

[8] Peiffer A.: Experimentelle Untersuchungen über mehrdimensionale Druckschwankungen bei Zugfahrten in Eisenbahntunneln Diplomarbeit TH–Karlsruhe 1994

[9] Woods W. A., Pope C. W.: On the range of validity of simplified one dimensional theories for calculating unsteady flows in railway tunnels. Proc. 3rd Int. Symp. on the Aerodynamics and Ventilation of Vehicle Tunnels 1979 Paper D2